From Cooperative Self-Assembly to Water-Soluble Supramolecular Polymers Using Coarse-Grained Simulations

From Cooperative Self-Assembly to Water-Soluble Supramolecular Polymers Using Coarse-Grained Simulations

*Davide Bochicchio and Giovanni M. Pavan**

Department of Innovative Technologies, University of Applied Sciences and Arts of Southern Switzerland, Galleria 2, Via Cantonale 2c, CH-6928 Manno, Switzerland

giovanni.pavan@supsi.ch

KEYWORDS. Supramolecular polymer, self-assembly, coarse-grained simulation, MARTINI force-field, 1,3,5-benzenetricarboxamide (BTA), cooperative polymerization, order amplification

ABSTRACT

Supramolecular polymers, formed via non-covalent self-assembly of elementary monomers, are extremely interesting for their dynamic bioinspired properties. In order to understand their behavior it is necessary to access their dynamics while maintaining high-resolution in the treatment of the monomer structure and monomer-monomer interactions, which is typically a difficult task, especially in aqueous solution. Focusing on 1,3,5-benzenetricarboxamide (BTA) water-soluble supramolecular polymers, we have developed a transferable coarse-grained model that allows studying BTA supramolecular polymerization in water, while preserving remarkable consistency with the atomistic models in the description of the key interactions between the monomers (hydrophobic, H-bonding, etc.), self-assembly cooperativity and amplification of order into the growing fibers. This permitted us to monitor the emergence and amplification of order and of the key interactions into the growing BTA fiber (including H-bonding) during the dynamic polymerization process. Our molecular dynamics simulations provide a picture of a stepwise cooperative polymerization mechanism, where initial fast hydrophobic aggregation of the BTA monomers in water is followed by the slower reorganization of these disordered aggregates into ordered directional oligomers. Polymer growth then proceeds on a slower timescale. We challenged our models via comparison with the experimental evidences, capturing the effect of temperature variations and subtle changes in the monomer structure on the polymerization and on the properties of the fibers seen in the real systems. This work provides a multiscale spatiotemporal characterization of BTA self-assembly in water, and a useful platform to study a variety of BTA-based supramolecular polymers toward unprecedented structure-property relationships.

Supramolecular polymers, where the monomers are interconnected via non-covalent interactions, have recently received notable attention thanks to their dynamic and adaptive properties.[1–3] These self-assembled structures possess self-healing behavior, stimuli responsiveness and dynamic bio-inspired properties reminiscent of those of many natural materials, which make them extremely interesting for the creation of novel advanced materials for nano- and bio-applications.[4] While their behavior is encoded into the molecular structure of the monomers and in the monomer-monomer interactions, gaining deep understanding of the key factors controlling the assembly is a first fundamental step toward the rational design of supramolecular polymers with controllable properties.[5–7] However, due to the reduced size and dynamic behavior of the monomers, and to the limited contrast offered by these soft assemblies in solution, obtaining detailed understanding of the behavior of the supramolecular polymers at experimental level is extremely difficult, especially in water.[6–8] This produces a general lack of molecular-level insight into the factors controlling the self-assembly in the aqueous environment. A tool providing access to the dynamics of the supramolecular polymers, while at the same time maintaining high resolution in the description of the monomer structure and accuracy in the treatment of the key interactions governing the self-assembly, would constitute a remarkable advance in the field.

Among many reported examples,[9–19] 1,3,5-benzenetricarboxamide monomers (BTA)-based supramolecular polymers, in which the BTA monomers directionally self-assemble due to core stacking and 3-fold hydrogen bonding between the amides of the BTAs (Figure 1a-c), are ideally suited for fundamental studies on supramolecular polymers in different conditions.[20] However, the intrinsic hydrophobicity of the monomers hinders the experimental study of their

polymerization and depolymerization in water using, for example, organic solvents or temperature. Consequently, the factors/mechanisms leading the formation of these supramolecular polymers in water remains often inaccessible.

In this context, molecular simulations have recently emerged as an important tool to study BTA and other types of supramolecular polymers,[9,15,21–28] as well as 1D ordered stacks[29–32]. Previous computational studies based on density functional theory studied the cooperativity of inter-monomer H-bonding and dipole amplification in small BTA stacks in the gas-phase.[21,24,33] Stacks of BTA monomers with short side chains (up to C_6) in organic solvents (*e.g.*, nonane) have also been investigated by means of all-atom classical molecular dynamics (MD) simulations,[23] providing insights into the BTA assembly in intrinsically ordered conditions (*i.e.*, the apolar solvent and the semi-rigid nature of the monomers favor the ordered stacking of the BTA cores). However, when moving to water complexity greatly increases due to the structure and the dynamics of the water-soluble monomers (*e.g.*, Figure 1a,b) and to the importance of the hydrophobic effects. All-atom (AA) classical MD simulations of peptide amphiphilic supramolecular fibers in explicit water have been reported, providing a detailed picture of the structure and H-bonding in the fiber.[9] Recently, we also used AA-MD simulations to study BTA supramolecular polymers in aqueous solution.[26] Our model of infinite BTA fibers allowed to study the effect of a subtle point mutation into the monomer – *i.e.*, the addition of a single methyl group into the side chains of the BTAs, making the monomers chiral – on the supramolecular polymer.[26] The differences captured by our AA models in terms of assembly structure (helicity, etc.), stability, order and water penetration in the interior of the polymer were proven useful to rationalize differences in supramolecular dynamics seen in the experiments – *i.e.*, faster/slower monomer exchange with the solution in the achiral/chiral BTA polymers respectively.[26] More

recently, comparison of AA models of water-soluble BTA stacks composed of an increasing number of monomers to disordered BTA aggregates of the same size also allowed us to unravel the delicate modulation of the key monomer-monomer interactions involved in the growth of an ordered BTA supramolecular polymer in water.[27]

While atomistic models provided important insight into these complex supramolecular assemblies, these are still subject to some important limitations, especially concerning the space- and time-scales that can be effectively explored, distant from those necessary to access the mechanism of self-assembly and the dynamic behavior of the supramolecular polymers. To tackle these limitations, one strategy is to develop coarse-grained (CG) models for the self-assembling monomers. Notable efforts have been made in this direction, where the development of CG models allowed to simulate the spontaneous self-assembly of proteins,[34] carbohydrates,[35] surfactants,[36] polymers,[37,38] etc. into micelles,[39] vesicles (polymersomes,[40] liposomes,[41] etc.), tubes,[42] bilayers,[43] and supramolecular fibers,[25,28] to name a few. Different coarse-graining strategies have been tested, using well-known "general" CG force fields such as MARTINI[44,45] or SDK,[46] as well as others developed *ad hoc*.[28] For example, the group of Balasubramanian recently reported an *ad hoc* CG model for a BTA derivative with short (C_6) side chains to study BTA self-assembly in explicit nonane via CG-MD simulations.[28] The group of Schatz used the MARTINI force field to model the spontaneous aggregation of CG peptide amphiphilic monomers into supramolecular fibers in water, obtaining useful insight on the assembled structure[25] and self-assembly mechanism.[47] While *ad hoc* CG models might in principle allow for higher accuracy in the representation and treatment of a determined system, the use of a "general" CG force field like MARTINI holds the remarkable advantage of high transferability and many chemical functionalities/groups already available and tested,[34–36] which facilitates monomer customization.

This is fundamental when one wants to study many variants of self-assembling monomers aiming at building structure-property relationships.

Herein, we have developed a transferable CG model for water-soluble BTA supramolecular polymers based on the MARTINI force field, which allows studying BTA self-assembly in water in time while maintaining remarkable consistency with the AA models for what pertains to the description of the key interactions involved in the process, including the possibility of explicitly monitoring inter-BTA H-bonding. In this way, we obtain access to the mechanism of BTA self-assembly (structure and kinetics). We can capture the effect of subtle monomer modifications or changes in the surrounding conditions consistent with the experiments. This provides a versatile and ideal platform to understand how to customize the BTA monomers to control the properties of the water-soluble supramolecular polymers.

RESULTS AND DISCUSSION

Coarse-grained models for water-soluble BTA

The self-assembly and growth of BTA directional assemblies rely on a delicate modulation of hydrophobic, van der Waals and directional H-bonding interactions. Recently, by using all atom molecular dynamics (AA-MD) we have discussed in detail the role of H-bonding and H-bonding cooperativity on the growth of an ordered BTA supramolecular polymer in water.[27] Initially focusing on the same system (Figure 1a), herein our fist aim was to create a CG model for the BTA monomers capable to capture the key features of the atomistic (AA) models especially in terms of the behavior of the BTA in the aqueous solution, monomer-monomer interactions and cooperativity of the self-assembly. We decided to use the MARTINI coarse-grained force field[44,45] as a basis to build our CG models, which is a reliable choice for modeling the self-assembly of

various types of supramolecular structures in water,[25,48] and allows for facile implementation of the models in various conditions. Furthermore, this choice offers the intriguing opportunity to study the interaction between the supramolecular polymers CG models and bio-relevant assemblies such as lipid bilayers, etc.[37,38,49]

For what concerns the aromatic core and the side chains of the BTA of Figure 1a, composed of hydrophobic dodecyl spacers (C_{12}) and tetraethylene glycol (PEG) terminal units, we based on optimized MARTINI parameters reported recently (see methods).[36,50] The CG representation of the BTA amide groups constituted a key point in our parametrization. In fact, the directional nature of H-bonding poses a relevant challenge to the MARTINI scheme, where all interactions are typically represented by a non-directional Lennard-Jones (LJ) potential. Thus, we built two variants of our BTA CG models, differing only in the description of the amides. A first model, BTA-CG_c, includes an explicit treatment of the H-bonding between the CG beads representing the BTA amides (Figure 1d: AMD_c). Similar to what recently done by the group of Balasubramanian,[28] the AMD_c amide bead contains a dipole (two $\pm q$ charges) mimicking the rigid amide orientation and the directionality in the BTA-BTA H-bonding typical of AA models (see methods and SI for details). On the other hands, in the second model, BTA-CG_0, the amides (Figure 1d: AMD_0) are represented by a standard martini bead. In this simpler model, the BTA-BTA H-bonding is thus implicitly contained into the AMD_0-AMD_0 LJ interactions. Both AMD_c and AMD_0 beads have been optimized to reproduce at CG level the core+amides dimerization free-energy profiles in water seen at atomistic level (see methods and SI). According to the standard MARTINI procedure,[37] the bond parameters (distances and angles), identical in all BTA-CG models, have been then refined to reproduce the behavior of the atomistic monomers in water.

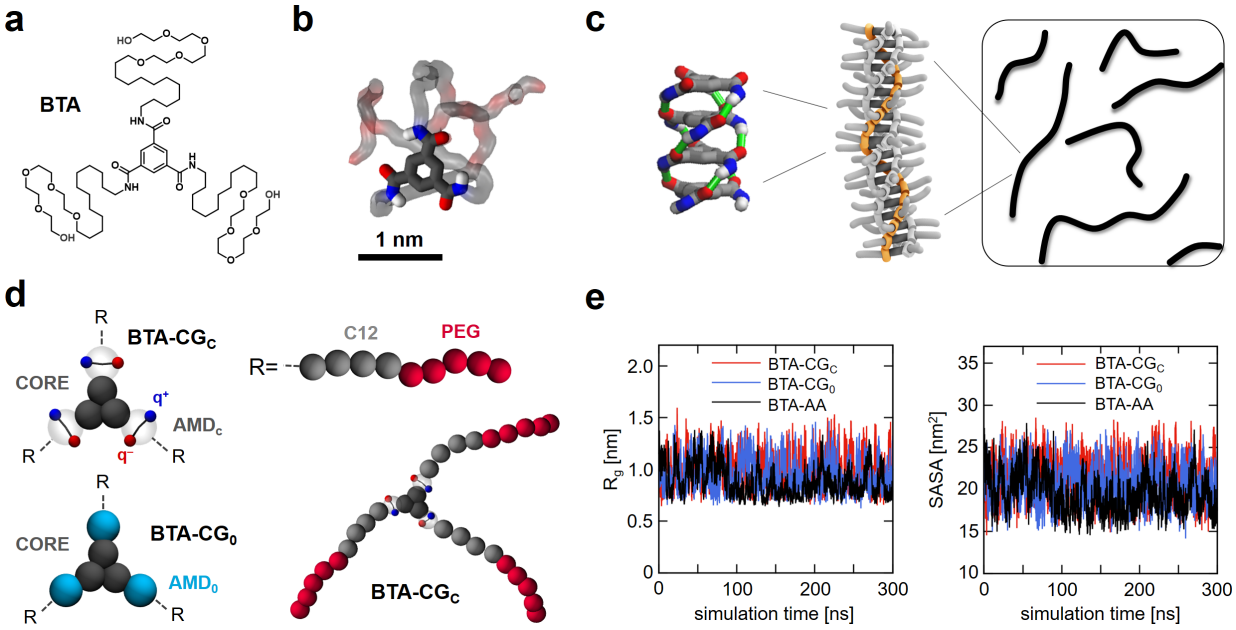

Figure 1. The reference water-soluble BTA monomer studied herein. (a) Chemical structure of the BTA. (b) Equilibrated atomistic model for the BTA in water.[26,27] (c) 1D self-assembly through core-core stacking and 3-fold H-bonding between the BTA amides leading to fiber growth. (d) MARTINI-based CG models for the core and side chains of the BTA. BTA-CG_c and BTA-CG_0 models differ in the description of the amides (respectively, with or without explicit description of inter-monomer H-bonding). (e) Consistency of the radius of gyration (R_g) and solvent accessible surface area (SASA) data at AA and CG level obtained from the MD simulations of a single BTA monomer in water.

At the single monomer level, the radius of gyration (R_g) and solvent accessible surface area (SASA) of the BTA-CG models were found to fit well with those of the BTA-AA one in explicit water (Figure 1e).[26,27] This demonstrates that both BTA-CG_c and BTA-CG_0 models well represent the behavior of the BTA monomer in water (correct hydrophobic/hydrophilic balance within the BTA structure), while the CG models show slightly faster dynamics than the AA one, as it is expected from a CG scheme.

Then, we explored the accuracy of the CG models in treating the interaction between the monomers in solution. Using metadynamics simulations,[51,52] we obtained the free-energies of dimerization for both the BTA-CG models and the BTA-AA one (considering the full BTA monomers in explicit water). These have been found identical in all cases (~-9±2 kcal mol^{-1}),

demonstrating the accuracy of the CG models in capturing the monomer-monomer interaction in the aqueous environment.

A fundamental point in such supramolecular polymers is the cooperativity of the self-assembly, where monomer addition becomes increasingly favorable while the polymer grows, eventually leveling off over a certain assembly size.[24,27] Recently, we have shown by means of AA-MD simulations how order emerges and is amplified into these BTA stacks due to augmentation of the key interactions in the assembly (hydrophobic and H-bonding).[27] We aimed at verifying the accuracy of our CG models in reproducing such an amplification of the inter-monomer interactions seen in the AA models. To this end, we started by building CG models for BTA stacks composed of 2, 3, 5, 7, 14 and 21 BTA monomers (Figure 2a) analogous to those simulated previously at atomistic level.[27] These systems have been equilibrated by means of CG-MD simulations (10 μs). We extracted relevant parameters indicative of the amplification of the key interactions (*i.e.*, hydrophobic and H-bonding) and of stacking order into the growing oligomers.

An indicator of the hydrophobic effects involved in the BTA self-assembly is the shrinkage of the SASA of the monomers due to aggregation in solution.[27] In particular, the ΔSASA, calculated as the difference between the average SASA of the BTAs in the different size assemblies and that of the monomer dissolved in solution ($\Delta SASA = SASA_{ass} - SASA_{monomer}$), provides indication of the strength of the hydrophobic effect. At the same time, the interacting $\pm q$ charges in the amides of the BTA-CG_c monomers (AMD_c), explicitly mimicking the inter-BTA H-bonding, allowed us to monitor the number of equivalent H-bonds per-BTA in the stacks and the associated H-bonding (electrostatic) energy. Finally, the level of order into the growing BTA oligomers can be accurately monitored from the radial distribution function of the BTA cores ($g(r)$) – *i.e.*, the

higher the *g(r)* peaks at stacking distances (*c*: closest neighbor, 2*c*: second closest, etc.), the higher the persistence/order in the stacking.[27]

We started by testing the BTA-CG$_c$ model in in both standard (W)[18,19] and polarizable (POL)[53] MARTINI water, where the partial charges in the POL beads might, in principle, interfere with the H-bonding between the BTAs (the $\pm q$ charges in the dipoles of AMD$_c$ have been opportunely adjusted to work correctly in the POL environment – see methods and SI). Up to the level of the 21-mers, the behavior of the BTA-CG$_c$ model in W and POL environments was found substantially invariant. Thus, from this point on we abandoned the use of the POL solvent as this was found to strongly slow down the CG-MD runs, hindering the possibility to explore larger sizes and longer timescales as it was expected from our CG models (results for the BTA-CG$_c$ model in POL solution are provided in the SI – Figure S4). On the other hands, the acceleration provided by our CG models in W water allowed to study way larger BTA systems.

Similar to what recently done at AA-level,[26,27] we built two pre-stacked systems (160* and 480*), composed of 160 and 480 initially extended BTA-CG$_c$ monomers replicating along the main fibers axis through periodic boundary conditions to form "infinite" BTA fibers. These systems, modeling the bulk of a BTA fiber, have been equilibrated by means of MD-CG simulations (Figure 4f: 480*, ten times bigger than the maximum size simulated at the atomistic level).[26,27] We also created two self-assembling systems composed of 160 and 300 BTA-CG$_c$ monomers initially dissolved in water, where the BTA monomers underwent spontaneous polymerization in water during the CG-MD runs (16 μs). All systems successfully reached the equilibrium with good stability during the CG-MD runs in the timescales of several microseconds (see methods and SI). Analogous pre-stacked and self-assembling BTA-CG$_0$ systems have been also built, simulated and analyzed for comparison.

As it can be inferred from Figure 2b, the shrinkage of the BTA SASA (ΔSASA) increases with the size of the assemblies, while this tends to a plateau for sizes greater than ~100 BTA. This cooperative behavior in the hydrophobic effects involved in the self-assembly is exactly the same observed recently at the atomistic level,[27] and it is directly imputable to a more efficient screening from the polar solvent of the hydrophobic parts of the BTA oligomers while the assembly size increases. Interestingly, BTA-CG_0 and BTA-CG_C behave in nearly identical way, demonstrating that both models capture the cooperativity of the hydrophobic effects in very similar way to the AA models.[27]

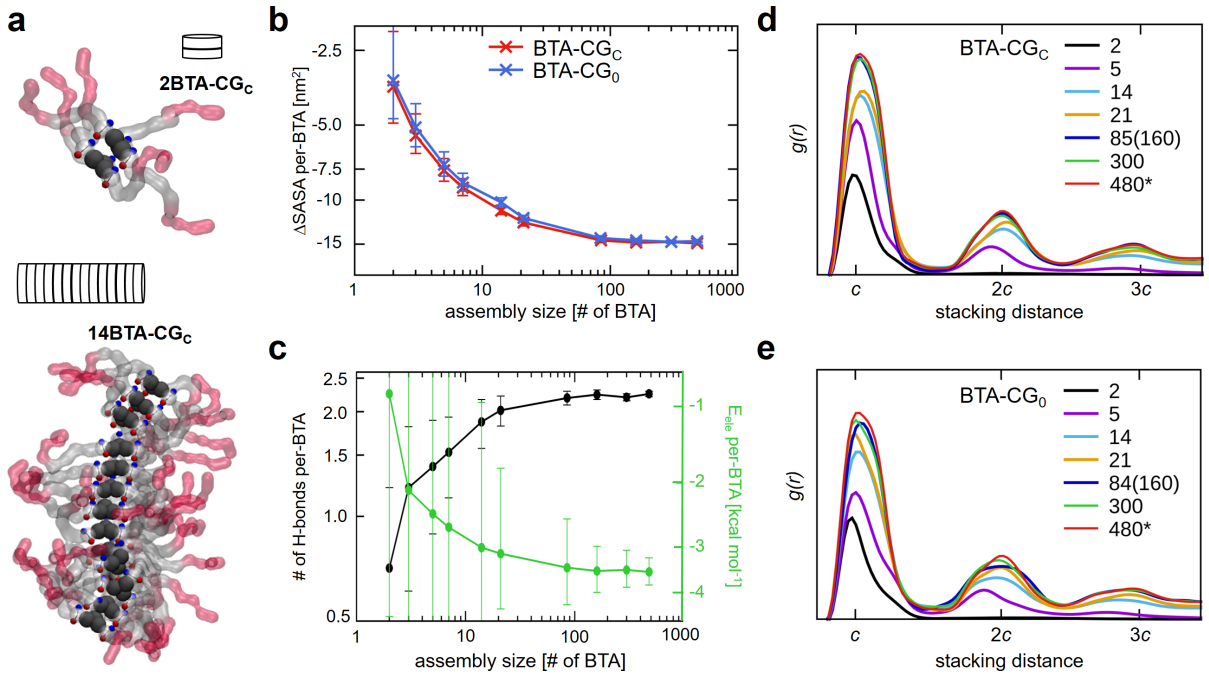

Figure 2. Self-assembly cooperativity: amplification of the key interactions and stacking order into the growing BTA oligomers. (a) BTA stacks of different size. (b) Hydrophobic effect: SASA variation (ΔSASA) per-BTA in the different size stacks as a function of the assembly size. (c) Average number of equivalent hydrogen bonds per-BTA and average H-bonding energy per-BTA as a function of the assembly size (in the BTA-CG_C systems). This amplification of the key interactions (hydrophobic and H-bonding) during polymer growth in the CG models is consistent with that recently seen at atomistic level.[27] (d,e) Amplification of stacking order into the growing BTA polymers. Radial distributions functions (*g(r)*) of the BTA cores in the different size systems for both BTA-CG_C and BTA-CG_0 models.

The BTA-CG_c model offers the unique opportunity to monitor the number of equivalent H-bonding and H-bonding energy as a function of the system size (see Figure 2c). The number of equivalent H-bonds per-BTA in the various simulated systems is seen to increase from ~0.7 for the dimer to, at saturation, ~2.2 for the largest systems (*e.g.*, 480* infinite fiber, etc.), identical to that recently found in the case of an AA infinite BTA fiber model in explicit water (composed of 48 BTAs).[27]

The average H-bonding energy per-BTA, directly extracted from the CG-MD simulations (electrostatic energy for the interaction between the $\pm q$ charges in the AMD_c groups), follows the same trend, becoming more and more favorable until approaching a plateau at ~-3.5 kcal mol^{-1}. Noteworthy, dividing the H-bonding energy for the average number of H-bonds per-BTA at saturation (2.2) we obtain an average energy per-single H-bond in water of ~-1.6 kcal mol^{-1}, in remarkable agreement with the energy of a single H-bond in aqueous solution for peptidic structures (-1.58 kcal mol^{-1}).[26,27,54] This demonstrates that our BTA-CG_c can correctly approximate the strength and the cooperativity of H-bonding into the growing BTA supramolecular polymer.

We also monitored the amplification of stacking order into the growing BTA-CG_c polymer.[27] Seen in Figure 2d, the height of the *g(r)* peaks increases with the size of the BTA-CG_c assemblies, reaching saturation in the largest systems. This behavior is again consistent with what recently observed at the atomistic level.[27] Furthermore, the fact that in the largest systems – both in the (i) bottom-up (160 and 300 dissolved monomers undergoing polymerization during the CG-MD runs) and (ii) top-down ones (*e.g.*, 480* and 160*: pre-stacked infinite fibers relaxed by means of MD-CG) – all relevant energetic and structural parameters converge to the same values clearly demonstrates that our CG models reliably reach the equilibrium within the CG-MD timescale of few tens of microseconds. This is an important advantage of CG models

compared to AA ones, where guaranteeing full equilibration and satisfactory sampling of these complex assemblies in water at atomistic resolution is not obvious.

Interestingly, the BTA-CG_0 systems were found to produce similar results than BTA-CG_c (Figure 2e), showing that also in the case of an implicit treatment of H-bonding, the self-assembly cooperativity and the amplification of order seen at AA level are substantially well reproduced. This has been rationalized as to be related to shape factors. In fact, while the rigid $\pm q$ dipoles in the BTA-CG_c model explicitly impart directionality to the AMD_c-AMD_c interaction, the presence itself of the aromatic BTA core and of the C_{12} spacers grafted on the two opposite sides respect to the AMD_0 center constrains to some extent the AMD_0-AMD_0 interactions on the plane perpendicular to the main axis of the BTA side chain (see SI – Figure S1).

Notably, from the structural point of view the final equilibrated cross-sectional radii for the 160* and 480* "infinite" CG fibers, and, for example, for the largest BTA oligomer spontaneously formed during the CG-MD simulation of the 160 self-assembling system (the 85-mer shown in Figure 3a) are found ranging ~2.6-2.9 nm, in good agreement with the experimental value extrapolated from SAXS measurements (3.1 ± 0.2 nm),[26] especially considering the structural approximations of the CG models.

Mechanism of BTA self-assembly in water

All data discussed above well demonstrate that CG models can accurately describe not only the behavior of the BTA monomers in water, but also the strength and cooperativity of the interactions between the BTAs and the amplification of stacking order into the growing BTA oligomers seen at AA level.[27] However, the acceleration guaranteed by the CG models opens up

the intriguing possibility to study the self-assembly of the BTA monomers in water in time, which is precluded to AA models due to the exaggerated structural complexity of the systems.

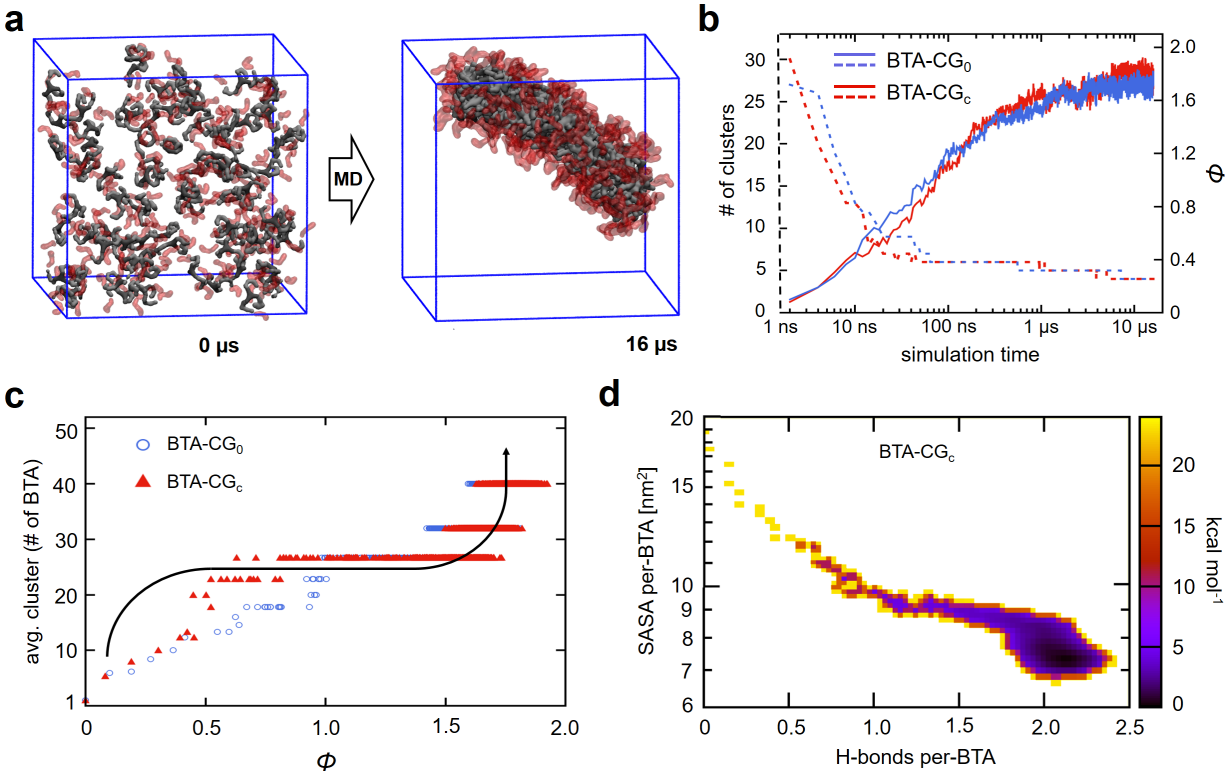

Figure 3. Mechanism of BTA self-assembly in water. (a) Starting and equilibrated (final) snapshots for the 160 BTA-CG$_c$ self-assembly system (for clarity, only the BTA monomers belonging to the largest cluster, a BTA 85-mer, spontaneously formed during the CG-MD, are shown). (b) Number of BTA clusters and order parameter Φ (core-core coordination) as a function of the CG-MD simulation time for the 160 BTA self-assembling systems (for both BTA-CG$_c$ and BTA-CG$_0$). (c) CG-MD trajectories as a function of the average cluster size (y axis) and Φ (x axis). (d) 2D self-assembly free-energy landscape for the BTA-CG$_c$ system as a function of the average number of H-bonds per-BTA and the average SASA per-BTA.

The molecular system composed of 160 BTA-CG$_c$ monomers initially dispersed in solution offers an interesting case study (Figure 3a). During the early steps of the CG-MD simulation (the first ~0-20 ns) the monomers in the system are seen to aggregate very rapidly, as demonstrated by the abrupt decrease in the number of BTA clusters present in the system (Figure 3b: dotted red line). The evolution of the order parameter Φ during the run (Figure 3b: solid red line)

indicates that up to ~30 ns of CG-MD simulation the BTA aggregates are still disordered. The Φ index represents the average coordination number between BTA cores, ranging 0 for dispersed BTAs to a maximum of 2 in theoretical perfect stacking condition (each BTA core has two coordinated neighbors). The Φ index increases considerably in time, reaching a maximum of ~1.8 after 16 μs of CG-MD. During this CG-MD simulation time, the largest BTA assembly spontaneously formed in solution is a fiber fragment with elongated shape – a BTA 85-mer, shown in Figure 3a. In this oligomer, the amplification of stacking order is already maximized, as demonstrated by the blue *g(r)* curve in Figure 2d (85(160)), superimposed to that of the infinite preformed 480* BTA fiber (in red). These data indicate that while the initial phase of BTA aggregation is very fast, the emergence and amplification of the stacking order into the oligomers proceeds at a much slower rate.

To better describe the BTA polymerization mechanism, we have plotted in Figure 3c the CG-MD trajectories of this system as a function of the average cluster size and of the order parameter Φ. Starting from the bottom-left corner in this plot (dispersed monomers), BTA self-assembly follows a sigmoidal pathway. This plot shows a stepwise polymerization process, which can be summarized as follows: first, (i) the monomers rapidly self-assemble forming disordered aggregates that, when reaching a certain size (~20-30 BTA in this case, but this clearly depends on the BTA concentration in the system), (ii) undergo structural reorganization evolving into ordered (stacked) BTA oligomers. (iii) Polymer growth then proceeds through the fusion of these ordered assemblies (discrete steps in the top-right region of the plot). This stepwise self-assembling process is consistent with recent hypotheses formulated on the base of thermodynamic and structural analyses of AA-MD simulations.[27] However, thanks to our CG

model it is possible to follow the supramolecular polymerization process in water in time during the simulations.

While Figure 3c allows identifying the steps involved in the BTA self-assembly, this provides no clear indication on their relative kinetics. As recently done for other self-assembling systems,[47,48] from the CG-MD simulation we obtained the free-energy landscape for the self-assembly process (see methods). The latter is represented as a function of the average SASA of the BTAs and the average number of H-bonds per-monomer. In Figure 3d, lighter colors (yellow) correspond to the most energetically unfavorable, and least visited, configurations, while darkest colors identify the most favorable, and most visited ones. Starting from the top-left in this plot, the monomers rapidly aggregate in the system following to hydrophobic effects (strong reduction of the SASA). In this phase, the H-bonding between the BTA cores is still reduced (<1 H-bond per-BTA). Then the BTA aggregates, rather than growing further in disordered way, optimize first their structure and augment the H-bonding, evolving into ordered stacks. Fiber elongation proceeds through the fusion of these ordered oligomers (bottom right free energy-minimum) on a slower timescale.

These data provide a multiscale picture (from monomer-monomer interactions to self-assembly, amplification of supramolecular order and fiber growth) of the BTA polymerization mechanism in water that is consistent with the AA models[27] and with the experiments. In fact, at experimental level, upon injection of molecularly dissolved BTA monomers from methanol into water an initial UV spectrum is observed, which changes with time into the final one obtained for the BTA polymers.[55] Furthermore, another recent experimental study showed that sugar-decorated BTA monomers form small aggregates at high temperatures, which upon cooling are then converted in time into supramolecular fibers.[56]

While obtaining a molecular-level perspective into the dynamic process of BTA supramolecular polymerization in water has until now represented an unsolved critical problem, all these data demonstrate the remarkable potential of our CG model in successfully dealing with this issue.

The BTA-CG_0 model produced similar results, forming large oligomers in solution found only slightly less ordered (Φ) than in BTA-CG_c, which can be imputed to the more directional nature of the attraction between AMD_c beads compared to AMD_0 (see SI – Figure S1). Noteworthy, while the BTA-CG_c model provides the remarkable opportunity to monitor the H-bonding between the BTA cores during the dynamic self-assembly process (quite unique at this level of accuracy), BTA-CG_0 offers a simpler, yet accurate, version of the model – a safer alternative when one wants to study, for example, the interaction of BTA supramolecular polymers with other bio-relevant molecular and supramolecular targets (proteins, DNA, lipid bilayer, etc.) easily implementable in the MARTINI framework.

Effect of structural modifications and temperature variations

Recently, experimental studies from the group of Meijer have shown that the BTA polymerization in water is extremely sensitive to changes in the hydrophobic/hydrophilic balance into the monomer structure.[8] While using C_{12} or C_{11} alkyl spacers in the side chains of the monomers produced nearly identical supramolecular fibers in aqueous solution, replacing the latters with C_{10} was found to inhibit the formation of BTA supramolecular polymers.[8]

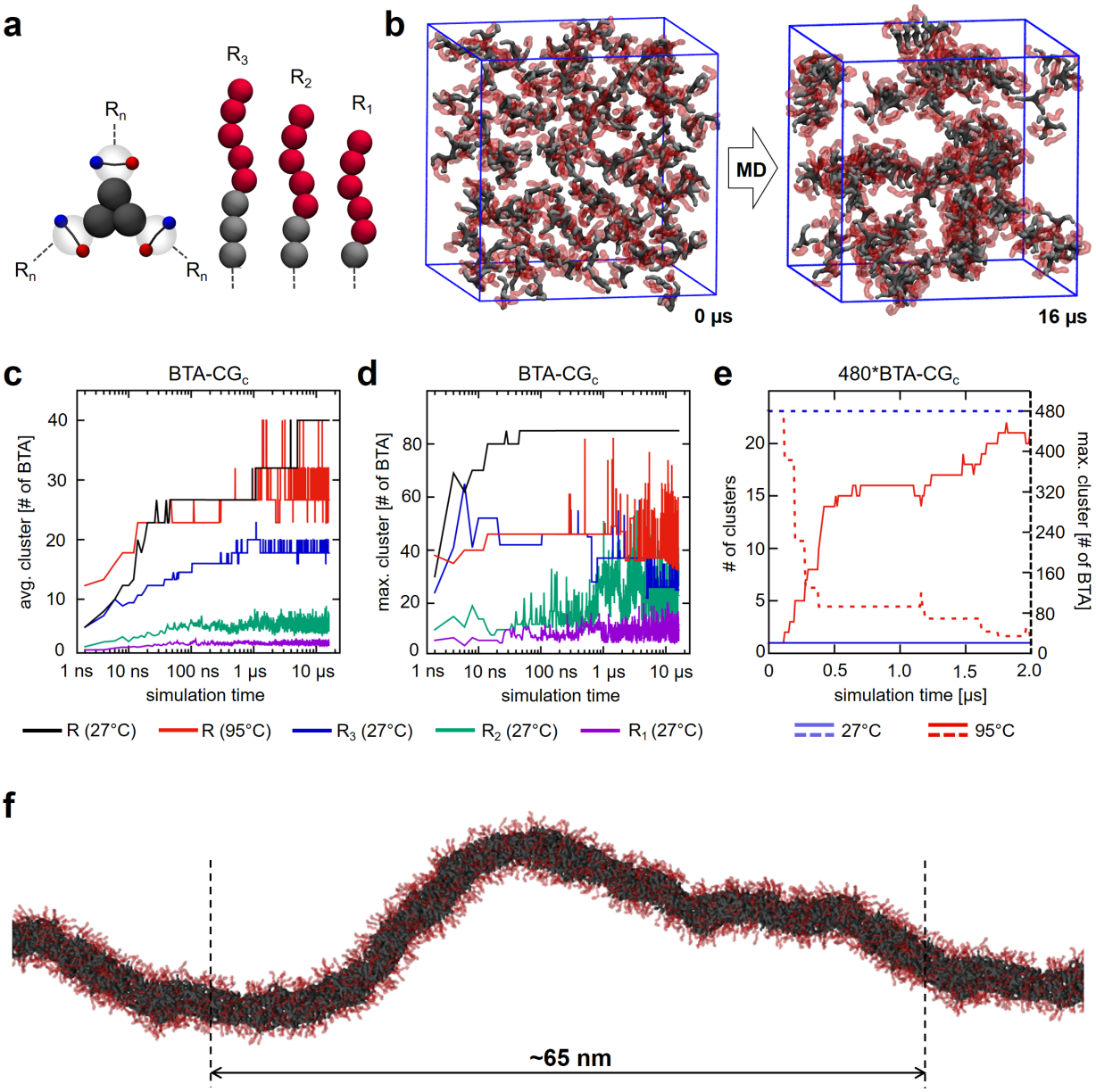

Figure 4. Effect of structural modifications in the monomers and temperature variations. (a) CG representation of BTA monomer variants where the alkyl hydrophobic spacers in the lateral chains have been systematically reduced. (b) Initial and final snapshots from the simulation of 160 C_6 BTA (R_2) self-assembling system in water. (c) Average cluster size and (d) size of the largest cluster formed along the CG-MD simulations of the different 160 self-assembling systems – *i.e.*, the standard C_{12} BTA and the three C_9, C_6 and C_3 BTA variants at room temperature (27 °C), and the standard C_{12} BTA at high temperature (95 °C). (d) Disassembly of the 480* C_{12} BTA "infinite" fiber during the CG-MD run when temperature is increased to 95°C – the number of clusters and the size of the largest BTA cluster in the system respectively increase and decrease during the simulation. (e) Equilibrated snapshot taken from the CG-MD simulation of the 480* BTA-CG_c infinite fiber model in water at room temperature.

We challenged our BTA CG models against these experimental evidences. To this end, compatibly with resolution allowed by our CG models, we built BTA-CG_c models with shorter hydrophobic spacers (containing respectively 3, 2 and 1 hydrophobic MARTINI beads, see Figure 4a and methods section) corresponding to C_9, C_6 and C_3 alkyl spacers. The same initial configuration used for the C_{12} BTA – 160 initially dispersed monomers in water – was used to build analogous systems for C_9, C_6 and C_3 BTA-CG_c, which underwent 16 μs of CG-MD simulation.

Our models demonstrated full consistency with the experimental evidences. In the C_6 and C_3 BTA-CG_c systems supramolecular polymerization was found completely hindered. Only very small BTA assemblies are spontaneously formed during the simulations (Figure 4b), as demonstrated by the reduced average and maximum sizes for the BTA clusters measured along the CG-MD (Figures 4c,d: green and purple). The C_9 BTA-CG_c system, at the threshold of the experimentally observed transition, is particularly interesting. Early during the CG-MD run this system attempts to grow a large oligomer – after ~3-5 ns, the latter has comparable size to that produced by C_{12} BTA-CG_c (Figure 4d, blue) –, but soon this turns out instable and disassembles ending into a size compatible with the average one for this system (Figure 4c, black). Thus, in our CG models, the polymerization of the C_9 BTA system is found inefficient. By contrast, in the case of C_{12} BTA-CG_c, supramolecular polymerization continues uniformly as demonstrated by the ascending evolution in time of the average cluster size (Figure 4c). Also, once the largest oligomer reaches the size of 85 BTAs (Figure 4d), it never disassembles during the 16 μs of CG-MD, indicating the stability of the assembly (further growth of longer fibers proceeds on a longer timescale). On the other hands, shortening the alkyl chains even by a single hydrophobic CG bead (3 carbon atoms) has strong effect on the ability of the systems to grow stable oligomers –

the maximum cluster size oscillates in a very dynamic way in C_9, C_6 and C_3 BTA-CG_c systems. Very similar results are obtained also in the case of the BTA-CG_0 model (see SI).

Recently, temperature-dependent experiments demonstrated that the C_{12} BTA fibers studied herein undergo a structural transition when the temperature in the system is increased above 60-80 °C. In such conditions, the BTA fibers, persistent at room temperature, disappear from the solution.[55] Thus, we decided to test the behavior of our systems at high temperature (95 °C, taking into consideration the level of accuracy that could be expected from our models).

We challenged the temperature sensitivity of our CG models from a double (i) bottom-up and (ii) top-down point of view. First, (i) starting from the same system with 160 initially dispersed C_{12} BTA-CG_c monomers, we analyzed the ability of the system to undergo polymerization at high temperature (Figure 4c,d: in red) and compared the data to those at room temperature (black). At 95 °C the C_{12} BTA-CG_c monomers initially aggregate, but polymerization is found unstable/ineffective and the clusters in the system cannot grow in stable way. Then, (ii) starting from the equilibrated 480* infinite BTA-CG_c fiber model obtained after 6μs of CG-MD (Figure 4f), we increased the temperature in the system to 95 °C and continued the simulation for other 2 μs at both high and room temperature for comparison. Shown in Figure 4e, the results of this simple test clearly demonstrate that the fiber is not stable and breaks into smaller clusters at high temperature. The number of clusters in the system (solid red line) increases rapidly from 1 to ~20 during the run, while at the same time the number of BTA monomers in the largest cluster in the system drops from the initial 480 (full fiber) to ~40 (red dotted line). On the contrary, the same fiber is found perfectly stable and persistent at 27° C, without a single fiber breakage during the whole CG-MD run (6+2 μs). Similar results are obtained also in the case of the BTA-CG_0 model (see SI – Figure S6).

While the sensitivity of the MARTINI force field to temperatures much higher than the bio-relevant ones is not obvious,[57] these results demonstrate that also in this sense our models are perfectly consistent with the experiments. Taken all together, these data prove that our CG models can reliably capture the effect of subtle modifications in the monomer structure[8] and changes in the external conditions[28] on the supramolecular BTA polymer. Moreover, these automatically provide demonstration of the transferability of these CG models, which can be readily modified (*e.g.*, changing the side chains, functional groups, etc.) to model variants of water-soluble BTA monomers in facile and reliable way.

Structure-property relationships

Recently, it has been shown by means of experiments and AA-MD simulations that other types of subtler structural modifications in the self-assembling monomers have important consequences on the monomer-monomer interactions and on the structure/dynamics of the supramolecular polymers.[26,27] In order to challenge further the transferability of our CG models, here we have built also two additional monomer variants and have compared them to C_{12} BTA. The first one is a recently reported 1,3,5-benzenetriester (BTE) derivative,[27] identical to C_{12} BTA, but having the amides replaced by ester groups (Figure 5a). While having nearly identical structure to C_{12} BTA, BTE monomers lack the ability to form the H-bonding network. It has been recently shown that these derivatives also form supramolecular fibers in water, albeit these are less persistent than their BTA analogs. In our CG model of the BTE (Figure 5a), we simply replaced the AMD beads of the BTA with the best-suited MARTINI beads to match the AA dimerization free-energy profile obtained for the BTE core+esters in explicit water (see methods and SI).

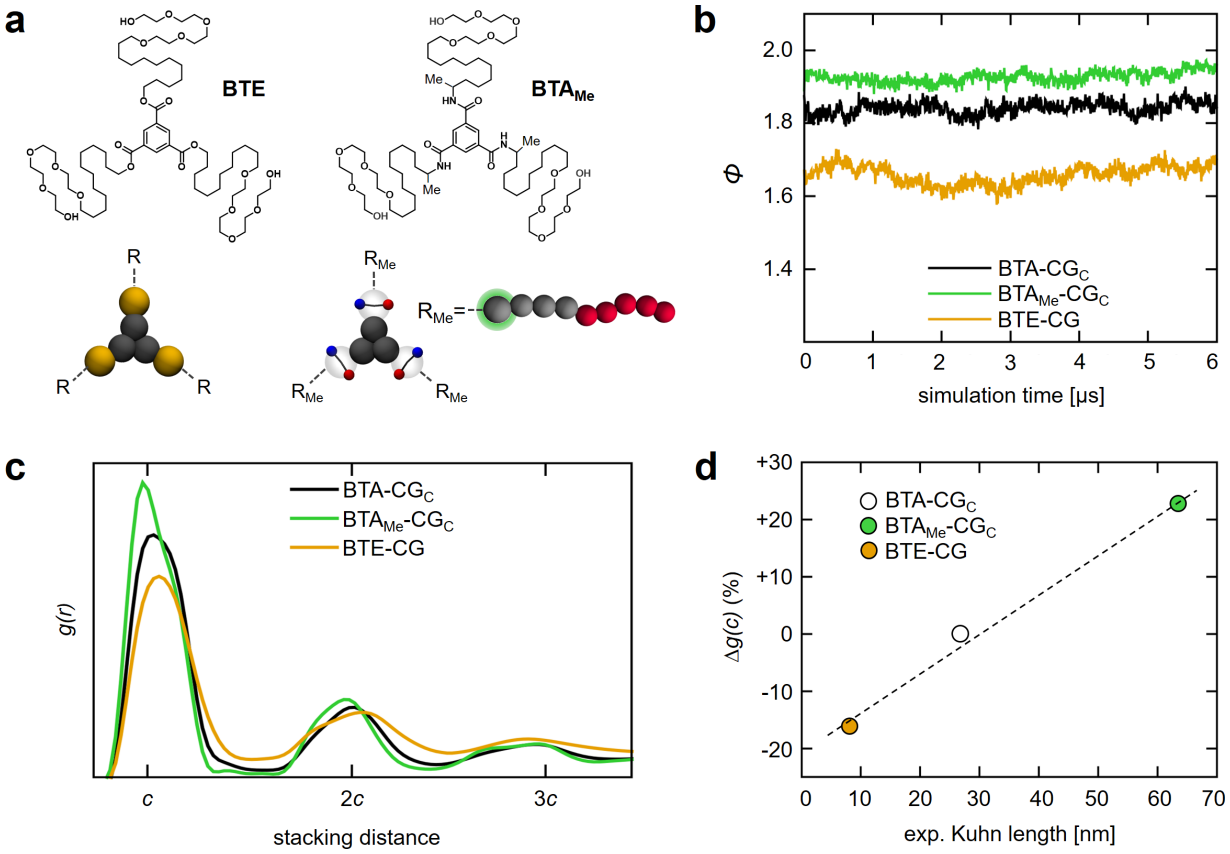

Figure 5. Transferability of the CG models and structure-property relationships. (a) Structure and CG models for the BTE and BTA_{Me} monomer variants. (b) Evolution of the order parameter Φ during the CG-MD simulations of BTA-CG_c, BTE-CG and BTA_{Me}-CG_c 480* infinite fiber models in water. (c) Radial distribution functions *g(r)* of the cores of the monomers extracted from the equilibrated phase of the CG-MD simulations for the three systems. (d) Linear trend between the % variation of *g(c)* (the height of the first *g(r)* peak, relative to direct core-core stacking) calculated respect to the BTA-CG_c system (set to 0 and here used as a reference) and the experimental Kuhn length of the three different fibers.[26,27]

The second monomer variant (BTA_{Me}), is again identical to C_{12}BTA except for the addition of a single carbon atom, a stereogenic methyl group, in the C_{12} alkyl spacers making the BTA_{Me} monomer chiral (Figure 5a).[26] While at experimental level BTA_{Me} and BTA produce nearly identical fibers in water, this single point mutation on the side chain of BTA_{Me} was recently found to increase the persistence and to reduce the dynamics (monomer exchange with the solution) of the supramolecular polymer compared to C_{12}BTA.[26] While our MARTINI model clearly cannot account for the effect of chirality, it can account for the steric hindrance introduced by the

addition of the methyl group into the side chain of BTA_{Me}. To this end, the first SC1 bead representing the first 3 carbon atoms in the C_{12} spacer of the BTA was simply replaced with a C1, the standard to represent 4 carbons (Figure 5a). Also in the case of BTA_{Me}, we built two CG model variants – *i.e.*, with (BTA_{Me}-CG_c) and without (BTA_{Me}-CG_0) explicit treatment of H-bonding.

Following to the same procedure adopted for the standard C_{12} BTA (see methods), we constructed and equilibrated BTE-CG and BTA_{Me}-CG_c infinite and initially extended 480* fiber models, which have been relaxed through 6 μs of CG-MD simulation. Both fibers were found stable during the runs, and showed similar macroscopic structure. However, when monitoring the order parameter Φ and the *g(r)* of the cores (Figures 5b,c), both indicators of stacking persistence and stability, we found relevant differences.

Compared to BTA-CG_c supramolecular polymer, the degree of ordering and stacking stability between the cores has been found respectively increased in BTA_{Me}-CG_c and decreased in BTE-CG fibers, fully consistent with our recent AA modeling of the same derivatives.[26,27] The height of the first *g(r)* peak (*g(c)*) is an indicator of the level of order and of the relative persistence of the stack,[26,27,31,58] which is in turn intrinsically related to the rigidity of the fiber, as a more persistent core-core stacking will intuitively produce less flexible fibers.[26,27] In Figure 4d we plotted the % of variation in *g(c)* obtained from the simulations of BTA_{Me}-CG_c and BTE-CG models compared to that of BTA-CG_c (set to 0 and used as a reference) against the experimental Kuhn length of the fibers.[26,27] This analysis produces remarkable linear trend between the molecular features of the assembly as captured by our CG models (relative *g(c)* height) and macroscopic properties of the polymers (flexibility/rigidity) from the experiments (very similar results are obtained for the BTA-CG_0 and the BTA_{Me}-CG_0 models – see SI). This proves once more the consistency of our CG

models with the atomistic ones and with the experiments, and the transferability of these CG models. This is extremely useful to model a variety of BTA-based supramolecular materials in aqueous environment in facile way, which is fundamental to build structure-property relationships directly relating the structure of the monomer to the dynamic polymerization process and the properties of the supramolecular fibers.

CONCLUSIONS

In this work, we have developed a coarse-grained model for BTA derivatives that allows studying the dynamic self-assembly and BTA polymerization in water. Two versions of the BTA CG model have been developed and tested, both correctly capturing the strength and cooperativity of the self-assembly and the amplification of order into the growing polymer seen at atomistic level. While BTA-CG_c also allows explicit monitoring of inter-BTA H-bonding, particularly useful to understand the dynamic evolution of the key interactions involved in the polymerization process, BTA-CG_0 offers a simpler alternative to study the interaction of BTA-based assemblies with other supramolecular targets (lipid bilayer, proteins, DNA, etc.). Thanks to the advantages provided by these CG models, we could simulate large systems composed of hundreds of BTA monomers self-assembling into supramolecular polymers in water. In this way, we could access the mechanism and dynamics of BTA supramolecular polymerization while maintaining remarkably high precision in the description of the key interactions involved in the self-assembly (including directional H-bonding). This is rather unique for such complex monomers, which self-assembly in water is controlled by a delicate modulation of directional (H-bonding) and non-directional (hydrophobic) forces.

Our CG models show remarkable consistency with the experimental evidences from multiple points of view, demonstrating good sensitivity to temperature variations and the ability to capture the effect of subtle changes in the structure of the BTA monomers. This work provides a unique tool for fundamental studies on the dynamic behavior of these complex supramolecular materials in water. The structure-property relationships that will be possible to obtain thanks to this model will be extremely useful to understand how to design/customize the monomers to control the final properties of the supramolecular polymers.

METHODS

Creation and parametrization of the BTA-CG models. The AA molecular models for the BTA and BTE variants were taken from our previous MD works,[26,27] were these had been originally parametrized based on the general AMBER force field (GAFF)[59] and simulated in explicit TIP3P[60] water molecules. As a basis for our coarse-grained model for water-soluble BTA derivatives (Figures 1a and 5a) we have used the MARTINI force field.[44,45,57] The philosophy of the MARTINI force field is to map 2-4 heavy atoms into a single bead, preserving the thermodynamic properties of the mapped species. The different polarity of the beads is realized by a proper scaling of their LJ interactions. In the standard MARTINI scheme, 4 water molecules are mapped into a single polar MARTINI bead. The use of this force field allows a 4-fold reduction in the number of particles and a significant increase of the time step used in MD simulations (from 1-2 fs to 20-40 fs).

For what concerns the parametrization of the BTA CG models studied herein, we followed the standard MARTINI parametrization procedure.[37] The beads used for the CG monomer variants simulated in this work are detailed in Table 1. The aromatic core has been parametrized

according to the standard for aromatic rings (benzene).[50] The C_{12}-PEG side chains of the BTA (Figure 1b) have been parametrized based on recent literature.[36] In particular, while the hydrophilic part (PEG) relies on the latest improved MARTINI version for polyethylene glycol from Rossi et al.,[36] for the hydrophobic part (C_{12}) we opted for using 4 SC1 beads, instead of 3 C1 MARTINI beads.[36] Our preliminary tests demonstrated that the difference between the two options was negligible. Moreover, while slightly better preserving the native flexibility of the alkyl spacers in the BTA, this choice also provided us with more space for structural customization of the monomers (*i.e.*, comparison between CG-BTA and CG-BTA_{Me}, etc.) and resolution uniformity with the CG description of PEG. In the two BTA-CG_c and BTA-CG_0 models the MARTINI beads for the amide groups (AMD_c and AMD_0 respectively) have been parametrized differently. In BTA-CG_c we wanted to introduce a dipole (2 partial charges) in the AMD_c bead to model the directionality of H-bonding. However, at the same time we did not want to create a completely new CG bead in order to preserve the transferability of the MARTINI force field. To this end, we used the polarizable water MARTINI bead (POL),[53] containing two movable charges, and have adapted the latter to our scope. The AMD_c bead in BTA-CG_c maintains the LJ parameters of the POL bead, while the $\pm q$ charges have been constrained at a distance of 0.17 nm from the AMD_c center, with the $(-q)$-AMD_c-$(+q)$ angle set to 180° (effectively keeping the charges at 0.34 nm from each other). The value of q (*i.e.*, the dipole strength) has been optimized to reproduce the dimerization free-energy profile of two BTA core+amides in water at atomistic level (*i.e.*, q was set to 0.61 e for BTA-CG_c in standard (W) water, or to 0.32 e in polarizable (POL) MARTINI water – see SI). On the other hands, in the CG-BTA_0 model we simply chose for the AMD_0 bead the standard MARTINI bead that again best reproduced the dimerization free-energy profile for the BTA core+amides in water at AA

level (*i.e.*, a P3 bead – see Table 1). The dimerization free-energy profiles for both coarse-grained BTA-CG_C (in W and POL water) and BTA-CG_0 (only W water) core+amides systems, and for the atomistic BTA-AA counterpart (in explicit TIP3P[60] water molecules), have been obtained by means of metadynamics simulations,[51,52] using the inter-core distance between the two reduced monomers as collective variable (hills height: 0.05 kcal mol^{-1} – hills width: 0.02 nm – deposition rate: 500 time steps).

Table 1. MARTINI beads used in all BTA, BTE and BTA_{Me} CG models developed in this work (see Figures 1a and 5a).

BTA-CG_0/CG_C		**BTE-CG**		**BTA-CG_0/CG_C-Me**	
CORE	3 SC5[a]	CORE	3 SC5[a]	CORE	3 SC5[a]
AMD_0 AMD_C	P3 POL (q=0.61 e)[b]	ESTER	C5	AMD_0 AMD_C	P3 POL (q=0.61 e)[b]
C_{12}[c]	4 SC1	C_{12}	4 SC1	C_{12}	1 C1 + 3 SC1[d]
PEG	4 SP0 SPh for the terminal group[e]	PEG	4 SP0 SPh for the terminal group[e]	PEG	4 SP0 SPh for the terminal group[e]

[a]Standard MARTINI representation for aromatic rings (*e.g.*, benzene).[50] [b]The value of the $\pm q$ charges in BTA-CG_C model has been optimized to reproduce the dimerization free-energy profiles of the BTA cores+amides obtained at AA level (see SI). In standard MARTINI water (W) the best fitting was found for q = 0.61 e (q = 0.32 e in polar MARTINI water, POL). [c]C_9, C_6 and C_3 reduced BTA-CG analogous models have been created by reducing the number of SC1 beads in the alkyl spacers (to 3, 2 and 1 SC1 respectively). [d]The addition of the methyl group in the BTA_{Me} monomer was modeled in BTA_{Me}-CG_C (and BTA_{Me}-CG_0) by replacing the first SC1 bead with a C1 bead (accounting for one more carbon). [e]Parameters for PEG were taken from the latest optimized PEG MARTINI parameters reported by Rossi et al.[36]

The errors in the free-energy profiles (see SI) for the AA and CG systems have been calculated averaging multiple free-energy profiles (6-10 depending on the system) taken at different times after convergence of a single metadynamics run.[61]

All bonded terms in the CG models of the BTA monomers (distances and angles potentials) have been refined in such a way to reproduce the distributions obtained from the AA-MD (see SI). The MD simulations of the individual CG monomers in water demonstrated very good agreement with the AA-MD for what pertains to the monomer behavior in water (R_g and SASA data in Figure 1c,d). Moreover, additional metadynamics simulations of BTA dimerization in water (accounting for the full BTA monomers) at both AA and CG levels provided identical dimerization free-energies in all cases (ΔG~-9±2 kcal mol^{-1}), not far from the ΔG~-13±3 kcal mol^{-1} recently obtained for the same BTA-AA dimer in water via more approximated MMPBSA analyses.[27]

Simulation and analysis. All CG-MD simulations have been carried out in NPT conditions (constant N: number of particles, P: pressure and T: temperature during the run) using the GROMACS 5.1.2 software[62,63] and using a 20 fs time step, except that for the simulations performed at 95° C, for which the time step was decreased to 10 fs. For the Metadynamics[51,52] simulations used to compare the dimerization free-energy profiles between the CG and AA models, we used the PLUMED 2 plugin.[64] In all simulations the systems were weakly coupled to external temperature and pressure baths using respectively the V-rescale[65] thermostat and the Parrinello-Rahman[66] barostat. The temperature was kept at 27 °C (95 °C for the simulations at high temperature) with a coupling constant of 2.0 ps. The pressure in the system was maintained at 1 atm with a coupling constant of 8 ps. All the simulated systems used isotropic pressure scaling, except for the 160* and 480* infinite fibers, for which we used semi-isotropic pressure

scaling due to the directional nature of the solutes.[26,27] For electrostatic and van der Waals (vdW) interactions, in all CG systems in W water we used a straight cutoff (1.1 nm) and potential modifiers, to better perform together with the Verlet neighbor list scheme.[67] The particle mesh Ewald (PME)[68] approach was used to treat the long-range electrostatic effects in those systems in POL water (the effect of using PME has been preliminarily tested also in the BTA-CG_C systems in W water, but in these cases no appreciable differences have been noted compared to the straight cutoff scheme). Details on the 45 molecular systems modeled and simulated in this study are provided in the SI.

Analysis of the simulations has been performed mainly using the GROMACS suite built-in facilities. For example, we used the *gmx clustsize* tool to follow in time the self-assembly process in terms of number of aggregates, average aggregate size and size of the largest aggregate present in solution, *gmx minidist* to calculate the order parameter Φ as the average coordination of the BTA cores, etc. The *g(r)* profiles, reported in Figures 2 and 5 as normalized for the volume of the spherical cell to compare between different size systems, have been obtained using *gmx rdf*. The free-energy landscape, represented in Figure 3e as a function of the average number of equivalent H-bonds and the average solvent-accessible surface area (SASA) per-BTA monomer, is useful to infer on how the self-assembly evolves in time, and it has been constructed from the CG-MD trajectory using with the method of histograms.[47,48]

ASSOCIATED CONTENT

Supporting Information. Details of all simulated systems, details and analyses for CG parametrization and additional modeling results. The following material is available free of charge (PDF).

AUTHOR INFORMATION

Corresponding Author

*Giovanni M. Pavan. Department of Innovative Technologies, University of Applied Sciences and Arts of Southern Switzerland, Galleria 2, Via Cantonale 2c, CH-6928 Manno, Switzerland. Email: giovanni.pavan@supsi.ch

ACKNOWLEDGMENT

The authors acknowledge the support from the Swiss National Science Foundation (SNSF grant 200021_162827 to GMP).

ABBREVIATIONS

1,3,5-benzenetricarboxamide (BTA); coarse-grained (CG); all-atom (AA); molecular dynamics (MD); 1,3,5-benzenetriester (BTE); polyethylene glycol (PEG)

REFERENCES

(1) Yang, L.; Tan, X.; Wang, Z.; Zhang, X. Supramolecular Polymers: Historical Development, Preparation, Characterization, and Functions. *Chem. Rev.* **2015**, *115*, 7196–7239.

(2) De Greef, T. F. A.; Smulders, M. M. J.; Wolffs, M.; Schenning, A. P. H. J.; Sijbesma, R. P.; Meijer, E. W. Supramolecular Polymerization. *Chem. Rev.* **2009**, *109*, 5687–5754.

(3) De Greef, T. F. A.; Meijer, E. W. Materials Science: Supramolecular Polymers. *Nature* **2008**, *453*, 171–173.

(4) Aida, T.; Meijer, E. W.; Stupp, S. I. Functional Supramolecular Polymers. *Science* **2012**,

335, 813–817.

(5) Krieg, E.; Bastings, M. M. C.; Besenius, P.; Rybtchinski, B. Supramolecular Polymers in Aqueous Media. *Chem. Rev.* **2016**, *16*, 2414–2477.

(6) Fu, I. W.; Markegard, C. B.; Chu, B. K.; Nguyen, H. D. Role of Hydrophobicity on Self-Assembly by Peptide Amphiphiles via Molecular Dynamics Simulations. *Langmuir* **2014**, *30*, 7745–7754.

(7) Paramonov, S. E.; Jun, H. W.; Hartgerink, J. D. Self-Assembly of Peptide-Amphiphile Nanofibers: The Roles of Hydrogen Bonding and Amphiphilic Packing. *J. Am. Chem. Soc.* **2006**, *128*, 7291–7298.

(8) Leenders, C. M. A.; Baker, M. B.; Pijpers, I. A. B.; Lafleur, R. P. M.; Albertazzi, L.; Palmans, A. R. A.; Meijer, E. W. Supramolecular Polymerisation in Water; Elucidating the Role of Hydrophobic and Hydrogen-Bond Interactions. *Soft Matter* **2016**, *12*, 2887–2893.

(9) Lee, O. S.; Stupp, S. I.; Schatz, G. C. Atomistic Molecular Dynamics Simulations of Peptide Amphiphile Self-Assembly into Cylindrical Nanofibers. *J. Am. Chem. Soc.* **2011**, *133*, 3677–3683.

(10) Muylaert, D. E. P.; van Almen, G. C.; Talacua, H.; Fledderus, J. O.; Kluin, J.; Hendrikse, S. I. S.; van Dongen, J. L. J.; Sijbesma, E.; Bosman, A. W.; Mes, T.; *et al*. Early in-Situ Cellularization of a Supramolecular Vascular Graft Is Modified by Synthetic Stromal Cell-Derived Factor-1α Derived Peptides. *Biomaterials* **2016**, *76*, 187–195.

(11) Cui, H.; Webber, M. J.; Stupp, S. I. Self-Assembly of Peptide Amphiphiles: From

Molecules to Nanostructures to Biomaterials. *Biopolymers* **2010**, *94*, 1–18.

(12) Li, J.; Loh, X. J. Cyclodextrin-Based Supramolecular Architectures: Syntheses, Structures, and Applications for Drug and Gene Delivery. *Adv. Drug Deliv. Rev.* **2008**, *60*, 1000–1017.

(13) Appel, E. A.; Loh, X. J.; Jones, S. T.; Biedermann, F.; Dreiss, C. A.; Scherman, O. A. Ultrahigh-Water-Content Supramolecular Hydrogels Exhibiting Multistimuli Responsiveness. *J. Am. Chem. Soc.* **2012**, *134*, 11767–11773.

(14) Neirynck, P.; Brinkmann, J.; An, Q.; van der Schaft, D. W. J.; Milroy, L.-G.; Jonkheijm, P.; Brunsveld, L. Supramolecular Control of Cell Adhesion via Ferrocene-cucurbit[7]uril Host-Guest Binding on Gold Surfaces. *Chem. Commun.* **2013**, *49*, 3679–3681.

(15) Garzoni, M.; Cheval, N.; Fahmi, A.; Danani, A.; Pavan, G. M. Ion-Selective Controlled Assembly of Dendrimer-Based Functional Nanofibers and Their Ionic-Competitive Disassembly. *J. Am. Chem. Soc.* **2012**, *134*, 3349–3357.

(16) Astachov, V.; Garzoni, M.; Danani, A.; Choy, K.-L.; Pavan, G. M.; Fahmi, A. In Situ Functionalization of Self-Assembled Dendrimer Nanofibers with Cadmium Sulfide Quantum Dots through Simple Ionic-Substitution. *New J. Chem.* **2016**, *40*, 6325–6331.

(17) Bastings, M. M. C.; Koudstaal, S.; Kieltyka, R. E.; Nakano, Y.; Pape, A. C. H.; Feyen, D. A. M.; van Slochteren, F. J.; Doevendans, P. A.; Sluijter, J. P. G.; Meijer, E. W.; *et al*. A Fast pH-Switchable and Self-Healing Supramolecular Hydrogel Carrier for Guided, Local Catheter Injection in the Infarcted Myocardium. *Adv. Healthc. Mater.* **2014**, *3*, 70–78.

(18) Wang, J.; Xia, H.; Zhang, Y.; Lu, H.; Kamat, R.; Dobrynin, A. V.; Cheng, J.; Lin, Y.

Nucleation-Controlled Polymerization of Nanoparticles into Supramolecular Structures. *J. Am. Chem. Soc.* **2013**, *135*, 11417–11420.

(19) Matson, J. B.; Zha, R. H.; Stupp, S. I. Peptide Self-Assembly for Crafting Functional Biological Materials. *Curr. Opin. Solid State Mater. Sci.* **2011**, *15*, 225–235.

(20) Cantekin, S.; de Greef, T. F. A.; Palmans, A. R. A. Benzene-1,3,5-Tricarboxamide: A Versatile Ordering Moiety for Supramolecular Chemistry. *Chem. Soc. Rev.* **2012**, *41*, 6125–6137.

(21) Filot, I. A. W.; Palmans, A. R. A.; Hilbers, P. A. J.; Van Santen, R. A.; Pidko, E. A.; De Greef, T. F. A. Understanding Cooperativity in Hydrogen-Bond-Induced Supramolecular Polymerization: A Density Functional Theory Study. *J. Phys. Chem. B* **2010**, *114*, 13667–13674.

(22) Bejagam, K. K.; Kulkarni, C.; George, S. J.; Balasubramanian, S. External Electric Field Reverses Helical Handedness of a Supramolecular Columnar Stack. *Chem. Commun.* **2015**, *51*, 16049–16052.

(23) Bejagam, K. K.; Fiorin, G.; Klein, M. L.; Balasubramanian, S. Supramolecular Polymerization of Benzene-1,3,5-Tricarboxamide: A Molecular Dynamics Simulation Study. *J. Phys. Chem. B* **2014**, *118*, 5218–5228.

(24) Kulkarni, C.; Reddy, S. K.; George, S. J.; Balasubramanian, S. Cooperativity in the Stacking of Benzene-1,3,5-Tricarboxamide: The Role of Dispersion. *Chem. Phys. Lett.* **2011**, *515*, 226–230.

(25) Lee, O. S.; Cho, V.; Schatz, G. C. Modeling the Self-Assembly of Peptide Amphiphiles

into Fibers Using Coarse-Grained Molecular Dynamics. *Nano Lett*. **2012**, *12*, 4907–4913.

(26) Baker, M. B.; Albertazzi, L.; Voets, I. K.; Leenders, C. M. a; Palmans, A. R. a; Pavan, G. M.; Meijer, E. W. Consequences of Chirality on the Dynamics of a Water-Soluble Supramolecular Polymer. *Nat. Commun*. **2015**, *6*, 6234.

(27) Garzoni, M.; Baker, M. B.; Leenders, C. M. A.; Voets, I. K.; Albertazzi, L.; Palmans, A. R. A.; Meijer, E. W.; Pavan, G. M. Effect of H-Bonding on Order Amplification in the Growth of a Supramolecular Polymer in Water. *J. Am. Chem. Soc*. **2016**, *138*, 13985–13995.

(28) Bejagam, K. K.; Balasubramanian, S. Supramolecular Polymerization: A Coarse Grained Molecular Dynamics Study. *J. Phys. Chem. B* **2015**, *119*, 5738–5746.

(29) Chami, F.; Wilson, M. R. Molecular Order in a Chromonic Liquid Crystal: A Molecular Simulation Study of the Anionic Azo Dye Sunset Yellow. *J. Am. Chem. Soc*. **2010**, *132*, 7794–7802.

(30) Smulders, M. M. J.; Schenning, A. P. H. J.; Meijer, E. W. Insight into the Mechanisms of Cooperative Self-Assembly: The "sergeants-and-Soldiers" principle of Chiral and Achiral C 3-Symmetrical Discotic Triamides. *J. Am. Chem. Soc*. **2008**, *130*, 606–611.

(31) Beltrán, E.; Garzoni, M.; Feringán, B.; Vancheri, A.; Barberá, J.; Serrano, J. L.; Pavan, G. M.; Giménez, R.; Sierra, T. Self-Organization of Star-Shaped Columnar Liquid Crystals with a Coaxial Nanophase Segregation Revealed by a Combined Experimental and Simulation Approach. *Chem. Commun*. **2015**, *51*, 1811–1814.

(32) Feng, X.; Marcon, V.; Pisula, W.; Hansen, M. R.; Kirkpatrick, J.; Grozema, F.;

Andrienko, D.; Kremer, K.; Müllen, K. Towards High Charge-Carrier Mobilities by Rational Design of the Shape and Periphery of Discotics. *Nat. Mater.* **2009**, *8*, 421–426.

(33) Albuquerque, R. Q.; Timme, A.; Kress, R.; Senker, J.; Schmidt, H. W. Theoretical Investigation of Macrodipoles in Supramolecular Columnar Stackings. *Chem. Eur. J.* **2013**, *19*, 1647–1657.

(34) Monticelli, L.; Kandasamy, S. K.; Periole, X.; Larson, R. G.; Tieleman, D. P.; Marrink, S. J. The MARTINI Coarse-Grained Force Field: Extension to Proteins. *J. Chem. Theory Comput.* **2008**, *4*, 819–834.

(35) Lo, C. A.; Rzepiela, A. J.; Vries, A. H. De; Dijkhuizen, L.; Hu, P. H.; Marrink, S. J.; Lopez, C. A.; de Vries, A. H.; Hunenberger, P. H.; López, C. A.; *et al*. Martini Coarse-Grained Force Field: Extension to Carbohydrates. *J. Chem. Theory Comput.* **2009**, *5*, 3195–3210.

(36) Rossi, G.; Fuchs, P. F. J.; Barnoud, J.; Monticelli, L. A Coarse-Grained MARTINI Model of Polyethylene Glycol and of Polyoxyethylene Alkyl Ether Surfactants. *J. Phys. Chem. B* **2012**, *116*, 14353–14362.

(37) Rossi, G.; Monticelli, L.; Puisto, S. R.; Vattulainen, I.; Ala-Nissila, T. Coarse-Graining Polymers with the MARTINI Force-Field: Polystyrene as a Benchmark Case. *Soft Matter* **2011**, *7*, 698.

(38) Panizon, E.; Bochicchio, D.; Monticelli, L.; Rossi, G. MARTINI Coarse-Grained Models of Polyethylene and Polypropylene. *J. Phys. Chem. B* **2015**, *119*, 8209–8216.

(39) Velinova, M.; Sengupta, D.; Tadjer, A. V.; Marrink, S. J. Sphere-to-Rod Transitions of

Nonionic Surfactant Micelles in Aqueous Solution Modeled by Molecular Dynamics Simulations. *Langmuir* **2011**, *27*, 14071–14077.

(40) Percec, V.; Wilson, D. A.; Leowanawat, P.; Wilson, C. J.; Hughes, A. D.; Kaucher, M. S.; Hammer, D. A.; Levine, D. H.; Kim, A. J.; Bates, F. S.; *et al*. Self-Assembly of Janus Dendrimers into Uniform Dendrimersomes and Other Complex Architectures. *Science* **2010**, *328*, 1009–1014.

(41) Arnarez, C.; Uusitalo, J. J.; Masman, M. F.; Ingólfsson, H. I.; De Jong, D. H.; Melo, M. N.; Periole, X.; De Vries, A. H.; Marrink, S. J. Dry Martini, a Coarse-Grained Force Field for Lipid Membrane Simulations with Implicit Solvent. *J. Chem. Theory Comput*. **2015**, *11*, 260–275.

(42) Noguchi, H. Formation of Polyhedral Vesicles and Polygonal Membrane Tubes Induced by Banana-Shaped Proteins. *J. Chem. Phys*. **2015**, *143*, 243109.

(43) Marrink, S. J.; Mark, A. E. Molecular Dynamics Simulation of the Formation, Structure, and Dynamics of Small Phospholipid Vesicles. *J. Am. Chem. Soc*. **2003**, *125*, 15233–15242.

(44) Marrink, S. J.; de Vries, A. H.; Mark, A. E. Coarse Grained Model for Semiquantitative Lipid Simulations. *J. Phys. Chem. B* **2004**, *108*, 750–760.

(45) Marrink, S. J.; Risselada, H. J.; Yefimov, S.; Tieleman, D. P.; De Vries, A. H. The MARTINI Force Field: Coarse Grained Model for Biomolecular Simulations. *J. Phys. Chem. B* **2007**, *111*, 7812–7824.

(46) Shinoda, W.; Devane, R.; Klein, M. L. Zwitterionic Lipid Assemblies: Molecular

Dynamics Studies of Monolayers, Bilayers, and Vesicles Using a New Coarse Grain Force Field. *J. Phys. Chem. B* **2010**, *114*, 6836–6849.

(47) Yu, T.; Schatz, G. C. Free-Energy Landscape for Peptide Amphiphile Self-Assembly: Stepwise versus Continuous Assembly Mechanisms. *J. Phys. Chem. B* **2013**, *117*, 14059–14064.

(48) Guo, C.; Luo, Y.; Zhou, R.; Wei, G. Probing the Self-Assembly Mechanism of Diphenylalanine-Based Peptide Nanovesicles and Nanotubes. *ACS Nano* **2012**, *6*, 3907–3918.

(49) Rossi, G.; Barnoud, J.; Monticelli, L. Polystyrene Nanoparticles Perturb Lipid Membranes. *J. Phys. Chem. Lett.* **2014**, *5*, 241–246.

(50) De Jong, D. H.; Singh, G.; Bennett, W. F. D.; Arnarez, C.; Wassenaar, T. A.; Schäfer, L. V.; Periole, X.; Tieleman, D. P.; Marrink, S. J. Improved Parameters for the Martini Coarse-Grained Protein Force Field. *J. Chem. Theory Comput.* **2013**, *9*, 687–697.

(51) Barducci, A.; Bonomi, M.; Parrinello, M. Metadynamics. *Wiley Interdiscip. Rev. Comput. Mol. Sci.* **2011**, *1*, 826–843.

(52) Laio, A.; Parrinello, M. Escaping Free-Energy Minima. *Proc. Natl. Acad. Sci. U. S. A.* **2002**, *99*, 12562–12566.

(53) Yesylevskyy, S. O.; Schäfer, L. V.; Sengupta, D.; Marrink, S. J. Polarizable Water Model for the Coarse-Grained MARTINI Force Field. *PLoS Comput. Biol.* **2010**, *6*, 1–17.

(54) Sheu, S.-Y.; Yang, D.-Y.; Selzle, H. L.; Schlag, E. W. Energetics of Hydrogen Bonds in

Peptides. *Proc. Natl. Acad. Sci. U. S. A.* **2003**, *100*, 12683–12687.

(55) Leenders, C. M. A.; Albertazzi, L.; Mes, T.; Koenigs, M. M. E.; Palmans, A. R. A.; Meijer, E. W. Supramolecular Polymerization in Water Harnessing Both Hydrophobic Effects and Hydrogen Bond Formation. *Chem. Commun.* **2013**, *49*, 1963–1965.

(56) Leenders, C. M. A.; Jansen, G.; Frissen, M. M. M.; Lafleur, R. P. M.; Voets, I. K.; Palmans, A. R. A.; Meijer, E. W. Monosaccharides as Versatile Units for Water-Soluble Supramolecular Polymers. *Chem. Eur. J.* **2016**, *22*, 4608–4615.

(57) Marrink, S. J.; Tieleman, D. P.; Lyubartsev, A. P.; Laaksonen, A.; Reith, D.; Putz, M.; Muller-Plathe, F.; Izvekov, S.; Violi, A.; Voth, G. A.; *et al*. Perspective on the Martini Model. *Chem. Soc. Rev.* **2013**, *42*, 6801.

(58) Munkhbat, O.; Garzoni, M.; Raghupathi, K. R.; Pavan, G. M.; Thayumanavan, S. Role of Aromatic Interactions in Temperature-Sensitive Amphiphilic Supramolecular Assemblies. *Langmuir* **2016**, *32*, 2874–2881.

(59) Wang, J.; Wolf, R. M.; Caldwell, J. W.; Kollman, P. A.; Case, D. A. Development and Testing of a General Amber Force Field. *J. Comput. Chem.* **2004**, *25*, 1157–1174.

(60) Jorgensen, W. L.; Chandrasekhar, J.; Madura, J. D.; Impey, R. W.; Klein, M. L. Comparison of Simple Potential Functions for Simulating Liquid Water. *J. Chem. Phys.* **1983**, *79*, 926.

(61) Bochicchio, D.; Panizon, E.; Ferrando, R.; Monticelli, L.; Rossi, G. Calculating the Free Energy of Transfer of Small Solutes into a Model Lipid Membrane: Comparison between Metadynamics and Umbrella Sampling. *J. Chem. Phys.* **2015**, *143*, 144108.

(62) Berendsen, H. J. C.; van der Spoel, D.; van Drunen, R. GROMACS: A Message-Passing Parallel Molecular Dynamics Implementation. *Comput. Phys. Commun.* **1995**, *91*, 43–56.

(63) Abraham, M. J.; Murtola, T.; Schulz, R.; Páall, S.; Smith, J. C.; Hess, B.; Lindah, E. Gromacs: High Performance Molecular Simulations through Multi-Level Parallelism from Laptops to Supercomputers. *SoftwareX* **2015**, *1–2*, 19–25.

(64) Tribello, G. A.; Bonomi, M.; Branduardi, D.; Camilloni, C.; Bussi, G. PLUMED 2: New Feathers for an Old Bird. *Comput. Phys. Commun.* **2014**, *185*, 604–613.

(65) Bussi, G.; Donadio, D.; Parrinello, M. Canonical Sampling through Velocity Rescaling. *J. Chem. Phys.* **2007**, *126*, 14101.

(66) Parrinello, M.; Rahman, A. Polymorphic Transitions in Single Crystals: A New Molecular Dynamics Method. *J. Appl. Phys.* **1981**, *52*, 7182–7190.

(67) De Jong, D. H.; Baoukina, S.; Ingólfsson, H. I.; Marrink, S. J. Martini Straight: Boosting Performance Using a Shorter Cutoff and GPUs. *Comput. Phys. Commun.* **2016**, *199*, 1–7.

(68) Darden, T.; York, D.; Pedersen, L. Particle Mesh Ewald: An $N\cdot\log(N)$ Method for Ewald Sums in Large Systems. *J. Chem. Phys.* **1993**, *98*, 10089-10092.

SYNOPSIS (Word Style “SN_Synopsis_TOC”).